Chemical Geology 373 (2014) 106–114

Contents lists available at ScienceDirect

Chemical Geology

journal homepage: www.elsevier.com/locate/chemgeo

The effect of chloride on the adsorption of Hg onto three bacterial species

Sarrah Dunham-Cheatham [a,*], Brian Farrell [a], Bhoopesh Mishra [b], Satish Myneni [c], Jeremy B. Fein [a]

[a] Department of Civil & Environmental Engineering & Earth Sciences, University of Notre Dame, Notre Dame, IN 46556, USA
[b] Department of Physics, Illinois Institute of Technology, Chicago, IL 60616, USA
[c] Department of Geosciences, Princeton University, Princeton, NJ 08544, USA

ARTICLE INFO

Article history:
Received 30 September 2013
Received in revised form 18 February 2014
Accepted 22 February 2014
Available online 11 March 2014

Editor: Carla M Koretsky

Keywords:
Mercury
Chloride
Bacterial adsorption
Mercury speciation

ABSTRACT

Bulk adsorption and X-ray absorption spectroscopy experiments were conducted in order to investigate the ability of three bacterial species to adsorb Hg in the absence and presence of chloride from pH 2 to 10. Adsorption experiments were performed using non-metabolizing cells of *Bacillus subtilis*, *Shewanella oneidensis* MR-1, and *Geobacter sulfurreducens* suspended in a 0.1 M $NaClO_4$ electrolyte to buffer ionic strength. After equilibration, the aqueous phases were sampled and analyzed using inductively coupled plasma-optical emission spectroscopy (ICP-OES) for remaining Hg concentrations. The biomass from some experiments was analyzed using Hg X-ray absorption spectroscopy (XAS) to determine the binding environment of the Hg.

In both chloride-free and chloride-bearing systems, the three bacterial species studied exhibited similar adsorption behaviors. Chloride causes a dramatic shift in the adsorption behavior of each of the bacterial species. In the absence of chloride, each of the species exhibits maximum adsorption between pH 4 and 6, with decreasing but still significant adsorption with increasing pH from 6 to approximately 10. The extent of Hg adsorption in the chloride-free systems is extensive under all of the experimental conditions, and the concentration of adsorbed Hg exceeds the concentration of any individual binding site type on the cell envelope, indicating that binding onto multiple types of sites occurs even at the lowest pH conditions studied. Because binding onto an individual site type does not occur exclusively under any of the experimental conditions, individual stability constants for Hg–bacterial surface complexes cannot be determined in the chloride-free system. In the presence of chloride, all of the bacterial species exhibit minimal Hg adsorption below pH 4, increasing adsorption between pH 4 and 8, and slightly decreasing extents of adsorption with increasing pH above 8. The low extent of adsorption at low pH suggests that neutrally-charged $HgCl_2^0$ adsorbs only weakly. The increase in Hg adsorption above pH 4 is likely due to adsorption of Hg^{2+} and $HgCl(OH)^0$, and is limited by site availability and transformation to $Hg(OH)_2^0$ as pH increases. We use the adsorption data to determine stability constants of the Hg–, $HgCl(OH)$–, and $Hg(OH)_2$–bacterial cell envelope complexes, and the values enable estimations to be made for Hg adsorption behavior in bacteria-bearing geologic systems.

1. Introduction

Bacteria are present in soils and groundwater systems (Madigan et al., 2009), and adsorption onto bacterial cell envelope functional groups can affect the speciation, distribution and transport of heavy metals (Beveridge and Murray, 1976; Fortin and Beveridge, 1997; Ledin et al., 1999; Small et al., 1999; Daughney et al., 2002). Although the adsorption behaviors of a wide range of bacteria have been studied for a wide range of metals (e.g., Beveridge and Murray, 1976, 1980; Beveridge, 1989; Mullen et al., 1989; Fein et al., 1997, 2002; Borrok et al, 2004; Wu et al., 2006; Borrok et al, 2007), Hg has received less attention. Recent studies have found that proton-active sulfhydryl functional groups exist on the surface of bacterial cell envelopes (Guine et al., 2006; Mishra et al., 2009, 2010, 2011; Pokrovsky et al., 2012; Song et al., 2012). Many studies have demonstrated that Hg has a high binding affinity for sulfur compounds (Fuhr and Rabenstein, 1973; Blum and Bartha, 1980; Compeau and Bartha, 1987; Winfrey and Rudd, 1990; Benoit et al., 1999), and thus the adsorption of Hg to bacteria may be dominated by this type of binding. Due to the high affinity for this bond to form, bacteria have the potential to drastically affect the distribution, transport and fate of Hg in soil and groundwater systems.

Several studies have investigated the extent to which bacteria adsorb Hg (Chang and Hong, 1994; Ledin et al., 1997; Green-Ruiz, 2006; Mo and Lian, 2011), and all have observed that Hg is extensively removed from solution in the presence of bacteria under a range of experimental conditions, with Hg adsorption typically more extensive than that of other heavy metals (Hassen et al., 1998). The extent of metal adsorption to bacteria can be quantified using surface complexation models (SCMs). SCMs have been applied to a range of metal–bacteria

* Corresponding author.
E-mail address: dr.smdcheatham@gmail.com (S. Dunham-Cheatham).

http://dx.doi.org/10.1016/j.chemgeo.2014.02.030
0009-2541/

systems (e.g., Plette et al., 1996; Fein et al., 1997; Daughney and Fein, 1998; Cox et al., 1999; Fowle and Fein, 2000; Borrok et al., 2004), though only one study has used this approach to model Hg adsorption onto bacteria (Daughney et al., 2002). Daughney et al. (2002) measured Hg adsorption onto *Bacillus subtilis*, a Gram-positive bacterial species, as a function of bacteria-to-Hg ratio, pH, chloride concentration, bacterial growth phase and reaction time, and used the data to constrain stability constants for both chloride-free and chloride-bearing Hg–bacterial surface complexes. It is crucial to test the accuracy of these stability constants, and also to determine if other bacterial species exhibit similar Hg adsorption behavior. Adsorption represents the first, and rate controlling, step in the bioavailability of some metals to bacteria (Borrok et al., 2004; Sheng et al., 2011), so determining the accurate and precise stability constant values for Hg–bacterial surface complexes may be crucial for quantitative modeling of processes such as bacterial Hg-methylation and Hg toxicity.

In this study, we test the findings of Daughney et al. (2002) by measuring Hg adsorption onto *B. subtilis*, and we expand on the Daughney et al. (2002) study by measuring Hg adsorption behavior onto two other representative bacterial species. In addition to bulk adsorption measurements, we conducted X-ray absorption spectroscopy measurements to constrain the dominant Hg binding mechanisms. Bacterial adsorption experiments were conducted as a function of pH and chloride concentration using intact washed non-metabolizing bacterial cells. In addition to the experiments involving the Gram positive species *B. subtilis*, we conducted parallel experiments involving a common Gram negative bacterial species (*Shewanella oneidensis* MR-1) and a Gram negative species that is capable of Hg methylation (*Geobacter sulfurreducens*) in order to investigate if cell envelope type affects Hg adsorption and/or if methylating species exhibit unique Hg binding properties. We used the experimental results to construct surface complexation models that enable the calculation of Hg speciation and distribution in a wide range of natural and engineered bacteria-bearing systems.

2. Methods

2.1. Experimental methods

2.1.1. Bacterial growth and washing procedure

B. subtilis and *S. oneidensis* MR-1 cells were cultured and prepared aerobically following the procedures outlined in Borrok et al. (2007). Briefly, cells were maintained on agar plates consisting of trypticase soy agar with 0.5% yeast extract added. Cells for all experiments were grown by first inoculating a test-tube containing 3 mL of trypticase soy broth with 0.5% yeast extract, and incubating it for 24 h at 32 °C. The 3 mL bacterial suspension was then transferred to a 1 L volume of trypticase soy broth with 0.5% yeast extract for another 24 h on an incubator shaker table at 32 °C. Cells were pelleted by centrifugation at 8100 *g* for 5 min, and rinsed 5 times with 0.1 M $NaClO_4$.

G. sulfurreducens cells were cultured and prepared using a different procedure than described above. Cells were maintained in 50 mL of anaerobic freshwater basal media (ATCC 51573) at 32 °C (Lovely and Phillips, 1988). Cells for all experiments were grown by first inoculating an anaerobic serum bottle containing 50 mL of freshwater basal media, and incubating it for 5 days at 32 °C. Cells were pelleted by centrifugation at 8100 *g* for 5 min, and rinsed 5 times with 0.1 M $NaClO_4$ stripped of dissolved oxygen by bubbling a 85%/5%/10% $N_2/H_2/CO_2$ gas mixture through it for 30 min. After washing, the three types of bacteria used in this study were then pelleted by centrifugation at 8100 *g* for 60 min to remove excess water to determine the wet mass so that suspensions of known bacterial concentration could be created. All bacterial concentrations in this study are given in terms of g wet biomass per liter.

2.1.2. Bacterial potentiometric titrations

Surface complexation modeling requires determination of bacterial cell envelope site concentrations and acidity constants. These parameters have been determined previously for *B. subtilis* (Fein et al., 2005) and *S. oneidensis* MR-1 (Mishra et al., 2010), but they have not been determined for *G. sulfurreducens*. To obtain these values, four replicate potentiometric titrations of *G. sulfurreducens* cells (100 g/L) were conducted in 0.1 M $NaClO_4$ under a N_2 atmosphere with an automated burette assembly. The biomass suspension was prepared using washed biomass and 0.1 M $NaClO_4$ that was purged with N_2 gas for 30 min prior to the preparation of the suspension. The suspension pH was measured using a glass electrode filled with 4 M KCl that was standardized using commercially supplied pH standards. The titrations were performed by measuring the pH after each addition of aliquots of commercially supplied volumetric standard of 1.030 M NaOH or 1.048 M HCl to the suspension. Acid or base additions were made only after a maximum drift of 0.01 mV/s was attained.

The biomass suspension was titrated first with HCl to achieve a pH of ~2.0. The suspension was then titrated with NaOH to a pH of ~10.0. Titrations of the electrolyte solution only were performed before and after each biomass titration to verify mechanical accuracy and reproducibility.

2.1.3. Batch adsorption experiments

Aqueous Hg(II), chloride, and suspended bacteria parent solutions were prepared using circum-neutral 0.1 M $NaClO_4$ electrolyte solution (pH adjusted to 7.0 ± 0.5 using 0.2 M HNO_3 and/or 0.2 M NaOH), and either 1000 ppm Hg(II) or chloride (Cl^-) volumetric aqueous standards, or washed bacterial cells (as described above). The parent solutions were mixed together in the following order: an aliquot of chloride parent solution was added to a bacterial suspension, and then an aliquot of Hg(II) parent solution was added and the mixture was diluted with 0.1 M $NaClO_4$ to achieve a suspension with a log molality of Hg of −4.13, a log molality of chloride of −3.00, and either 0.2 g wet biomass/L (for the *B. subtilis* and *S. oneidensis* experiments) or 0.1 g wet biomass/L (for the *G. sulfurreducens* experiments). Chloride-free experiments were also conducted and prepared in an identical fashion, but excluding the chloride addition. Eight milliliter aliquots of the suspension were added to 20 Teflon reaction vessels and the pH of each aliquot was immediately adjusted to cover the pH range from 2 to 10, using 0.2 M HNO_3 and/or NaOH, and the vessels were placed on an end-over-end rotator for the duration of the experiment (2 h for *B. subtilis* and *G. sulfurreducens*, and 3 h for *S. oneidensis*). Kinetics experiments (data not shown) were conducted to determine the duration required for each system to attain steady-state conditions. The pH of each experiment was monitored and adjusted if necessary using 0.2 M HNO_3 and/or NaOH every 15 min throughout the duration of the experiment except during the last 30 min, during which the suspensions were undisturbed. At the completion of each experiment, the final pH of each solution was measured and the contents were filtered through a 0.2 μm PTFE syringe filter to remove the bacteria. The aqueous phase was collected and acidified using 15.8 N HNO_3 at a sample:acid ratio of 5 mL:8 μL and refrigerated pending aqueous Hg analysis. All experiments were performed under atmospheric, room temperature conditions. Three replicate experiments were conducted for each experimental condition.

2.1.4. Inductively-coupled plasma-optical emission spectroscopy (ICP-OES)

Ionic strength matrix-matched ICP-OES standards were prepared gravimetrically by diluting a commercially-supplied 1000 ppm Hg(II) aqueous standard with 0.1 M $NaClO_4$, and each standard was acidified using 8 μL of 15.8 N HNO_3 per 5 mL sample. The log molality of the Hg standards ranged from −6.30 to −4.05. The standards and samples were analyzed with a Perkin Elmer 2000DV ICP-OES at a wavelength of 253.652 nm within 2 days of collection. The set of standards was analyzed before and after all of the samples were analyzed, as well as

after every 15 samples, to check for machine drift. Analytical uncertainty, as determined by repeat analyses of the standards, was ±5.6%.

2.1.5. Synchrotron experiments: X-ray absorption spectroscopy (XAS)

Hg L_{III}-edge X-ray absorption near edge structure (XANES) and extended X-ray absorption fine-structure spectroscopy (EXAFS) measurements were performed at the MRCAT Sector 10-ID Beamline (Segre et al., 2000), Advanced Photon Source, at the Argonne National Laboratory. The continuous-scanning mode of the undulator was used with a step size of 0.5 eV and an integration time of 0.1 s per point to decrease the radiation exposure during a single scan. Additionally, measurements were made at different spots on the samples to further decrease the exposure time. Hg XAS measurements were conducted as outlined in Mishra et al. (2011).

Three Hg solutions, Hg-chloride, Hg-cysteine, and Hg-acetate, were utilized as standards for Hg XAS analyses. The Hg-chloride standard was prepared by adding mercuric chloride salt (Alfa-Aesar) to 18 MΩ ultrapure water and adjusting the pH to 3.0 ± 0.1 by adding appropriate amounts of 1 M or 5 M HNO_3 or NaOH. To prepare the Hg-cysteine standard, first an aqueous Hg standard was prepared from high-purity 5 mM dissolved Hg in 5% HNO_3. The pH of the solution was adjusted to pH 2.0 ± 0.1 by adding small aliquots of 5 M NaOH. Cysteine was added to this solution to achieve a Hg:cysteine ratio of 1:100. The pH of the Hg-cysteine standard was adjusted to 5.0 ± 0.1 by adding small aliquots of 1 M or 5 M NaOH. The Hg-acetate standard was prepared by adding mercuric acetate salt (Alfa-Aesar) to ultrapure water and adjusting the pH to 5.0 ± 0.1 by adding small aliquots of 1 M or 5 M NaOH.

To prepare the Hg XAS biomass samples, *S. oneidensis* MR-1 biomass was reacted with aqueous Hg by diluting a commercially-supplied 1000 mg L^{-1} Hg standard with a pH-adjusted 50 mg L^{-1} NaCl stock solution prepared in 0.1 M $NaClO_4$. The experimental conditions included log molalities of Hg of −5.00, −4.60, and −4.13 at both pH 5.50 ± 0.10 and 8.00 ± 0.10. The bacterial concentration in all experiments was 2 g L^{-1}, and each experimental condition was prepared either in the absence of chloride or in the presence of a log molality of chloride of −3.00. Reacted biomass samples were loaded into slotted Plexiglas holders that were subsequently covered with Kapton tape with a Kapton film sandwiched in between the tape and the Plexiglas to avoid direct contact of the sample with the tape adhesive. Samples were refrigerated until data collection. All measurements were conducted within 48 h of sample preparation.

The data were analyzed using the methods described in the UWXAFS package (Stern et al., 1995). Energy calibration between different scans was maintained by measuring Hg/Sn amalgam on the reference chamber concurrently with the fluorescence measurements of the biomass-bound Hg samples (Harris et al., 2003). The inflection point of the Hg L_{III}-edge (12.284 KeV) was used for calibration. Data processing and fitting were done with the ATHENA and ARTEMIS programs (Ravel and Newville, 2005). The data range used for Fourier transformation of the *k*-space data was 2.0–9.5 $Å^{-1}$. The Hanning window function was used with dk = 1.0 $Å^{-1}$. Fitting of each spectrum was performed in *r*-space, at 1.2–3.2 Å, with multiple *k*-weighting (k^1, k^2, k^3) unless otherwise stated. Lower χ^2_ν (reduced chi square) was used as the criterion for inclusion of an additional shell in the shell-by-shell EXAFS fitting procedure.

2.2. Thermodynamic modeling

We used a non-electrostatic surface complexation approach to model proton and Hg adsorption onto bacterial cell envelope functional groups (Fein et al., 1997, 2005). That is, we modeled the acidity of surface functional groups via deprotonation reactions:

$$R{-}A_iH^0 \Leftrightarrow R{-}A_i^- + H^+ \quad (1)$$

where *R* represents the cell envelope macromolecule to which each type of functional group, A_i, is attached. The distribution of protonated and deprotonated functional group sites can be quantified via mass action equations, such as:

$$K_i = \frac{[R{-}A_i^-]a_{H^+}}{[R{-}A_iH^0]} \quad (2)$$

where K_i represents an acidity constant, *a* represents the activity of the subscripted species, and the brackets represent the activities of surface sites in moles per liter of solution.

In applying this approach to modeling the surface acidity of bacteria, we implicitly assumed that the deprotonation of each type of functional group, A_i, can be represented as a single deprotonation of an organic acid. Because all of our experiments were conducted at the same ionic strength, we ignored potential ionic strength effects on the surface electric field, applying a non-electrostatic model to account for the titration and Hg adsorption data. Potentiometric titration experiments are essentially studies of proton adsorption and desorption, yet because the solvent contains the same element as is reacting with the surface of interest, it is impossible to apply a traditional mass balance approach. Instead, one must define a zero proton condition for the bacterial cell envelope, and account for changes in proton concentrations relative to that condition (e.g., Westall et al., 1995; Fein et al., 2005). After the approach by Fein et al. (2005), we chose fully protonated cell envelope sites to represent our zero proton condition, and we used FITEQL (Westall, 1982) to solve for the initial state of protonation in each titration (Westall et al., 1995).

As is discussed below, the extent of Hg adsorption that we observed in the chloride-free systems was too extensive to be able to isolate or model the extent of adsorption onto individual cell envelope sites. For the chloride systems, we model the observed adsorption as interactions between aqueous Hg species and deprotonated bacterial cell envelope sites:

$$Hg\,species^{+x} + R{-}A_i^- \Leftrightarrow (R{-}A_i)(Hg\,species)^{x-1} \quad (3)$$

where '$Hg\ species^{+x}$' represents the specific aqueous Hg species tested in each model, '$(R{-}A_i)(Hg\ species)^{x-1}$' represents the Hg–bacterial cell envelope complex, and *x* represents the charge of the aqueous Hg species. The mass action equation for Reaction 3 is:

$$Kads = \frac{\left[(R{-}A_i)(Hg\ \ species)^{(x-1)}\right]}{a(Hg\ \ species^{+x})[R{-}A_i^-]} \quad (4)$$

where K_{ads} is the thermodynamic equilibrium constant for Reaction 3, *a* represents the activity of the species in parentheses, and brackets represent concentrations in mol/L. Acid/base potentiometric titration data provide constraints on the number of site types, their K_i values and their site concentrations; Hg adsorption measurements conducted as a function of pH constrain the number of sites involved in Hg binding, the pH range of influence, and the stability constants for the important Hg–bacterial cell envelope complexes. We used the program FITEQL 2.0 (Westall, 1982) for the equilibrium thermodynamic modeling of the adsorption data, using the aqueous speciation equilibria and equilibrium constants given in Table S1, and using the program's activity coefficient calculations via the Davies equation.

3. Results & discussion

3.1. Potentiometric titrations

Potentiometric titrations of *G. sulfurreducens* biomass were performed in order to calculate site concentrations and pKa values for discrete proton-active cell envelope functional groups. *G. sulfurreducens* exhibits significant proton buffering behavior over the entire pH range

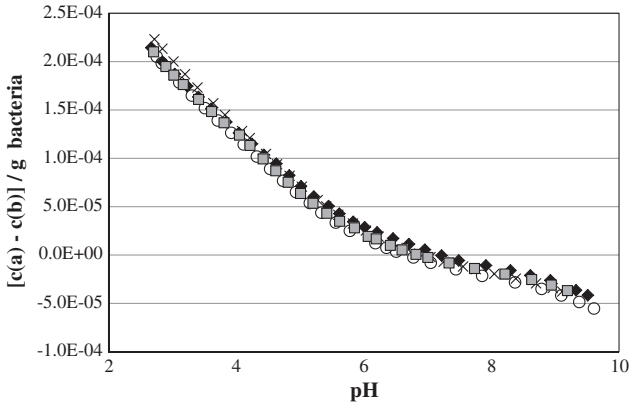

Fig. 1. Four replicate forward potentiometric titration of 100 g/L *G. sulfurreducens* in 0.1 M $NaClO_4$.

studied. Each of the four replicate *G. sulfurreducens* sets of titration data is depicted in Fig. 1. *G. sulfurreducens* exhibits a similar total buffering capacity $((C(a) - C(b) - [H^+] + [OH^-])/m_b)$ to that measured for other bacterial species. For example, between pH 3 and 9, *G. sulfurreducens* has a buffering capacity of $3.5 \pm 0.6 \times 10^{-4}$ mol/g (reported error represents 1σ uncertainty), compared to a value of 3.0×10^{-4} mol/g for *B. subtilis* (Fein et al., 2005), 3.1×10^{-4} for *S. oneidensis* MR-1 (Mishra et al., 2010), and 1.27×10^{-4} and 2.23×10^{-4} mol/g for *Acidiphilium acidophilum* and *Bacillus pseudofirmus*, respectively (Kenney and Fein, 2011). Borrok et al. (2005) observed that a wide range of bacterial species exhibit similar buffering behaviors, and our titration data demonstrate that *G. sulfurreducens* exhibits that same buffering behavior.

The potentiometric titration data were used to quantify the site concentrations and acidity constants for *G. sulfurreducens*. 1-, 2-, 3-, 4-, and 5-site models were tested in order to determine the number of proton-active surface site types on *G. sulfurreducens* cell envelopes needed to account for the observed buffering behavior. The addition of each additional site significantly lowered the V(Y) (variance) value from an average of 185.6 for the 1-site models of the 4 titrations to an average of 0.26 for the 4-site models (an ideal V(Y) value is 1). A 5-site model failed to converge for each set of titration data, indicating insufficient experimental data to constrain parameters for 5 site types. Fig. 2 shows a representative titration for *G. sulfurreducens* with the corresponding best fit 4-site model. The model yields an excellent fit to the observed buffering behavior across the pH range of the study. *G. sulfurreducens* has similar site concentrations and pKa values to *B. subtilis* and *S. oneidensis* MR-1 (Table 1), though *G. sulfurreducens* has the lowest concentration of total surface sites of the three species.

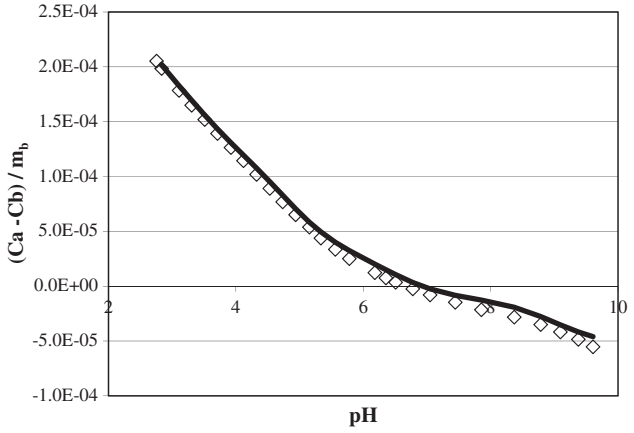

Fig. 2. Best fit 4-site model results (smooth curve) for one representative potentiometric titration of *G. sulfurreducens* (data points).

The presented site concentrations and pKa values in Table 1 represent the averages of the 4 individual forward titration model results, and are used as a basis for our Hg adsorption modeling.

3.2. Adsorption experiments

In the absence of chloride, the adsorption behavior as a function of pH is more complex than has been observed for other metal cations (e.g., Fein et al., 1997, 2001), with the extent of adsorption increasing from pH 2 to 4, and in general decreasing from 4 to 9 (Fig. 3). The extent of Hg adsorption that we observed is notable. In the chloride-free experiments, *B. subtilis*, *S. oneidensis* MR-1, and *G. sulfurreducens* adsorbed a maximum of approximately 2.0×10^{-4}, 3.0×10^{-4}, and 3.5×10^{-4} mol Hg per g (wet mass) of bacteria, respectively. In similar Hg adsorption experiments involving *B. subtilis* but conducted under much lower Hg loading conditions, Daughney et al. (2002) measured a maximum of only approximately 5.0×10^{-6} mol Hg per g (wet mass). Clearly, these bacteria exhibit a much higher capacity for Hg than was probed by the Daughney et al. (2002) experiments.

In the presence of chloride, the pH dependence of Hg adsorption that we observed differs dramatically from the typical behavior observed with metal cations, even though the dominant aqueous Hg species are neutral or negatively charged. There is only a small extent of adsorption below pH 4, with adsorption increasing slightly from pH 2 to 4; the extent of adsorption increases more markedly with increasing pH between approximately pH 4 and 8, and the extent of adsorption decreases slightly with increasing pH above pH 8. The addition of chloride to the experimental system significantly decreases the extent of Hg adsorption onto the bacteria under low pH conditions relative to the chloride-free system, and does not markedly affect the extent of Hg adsorption above pH 6 (Fig. 4).

In general, the bacterial species tested exhibit broadly similar bulk adsorption behaviors in the absence and presence of chloride, although there are some differences. In the chloride-free system, although experimental uncertainties are relatively high, in the mid-pH range tested, *G. sulfurreducens* removes more Hg from solution than *S. oneidensis* MR-1 which removes more than *B. subtilis*; the differences between species are less under lower and higher pH conditions. In the chloride systems, *B. subtilis* and *G. sulfurreducens* remove nearly identical amounts of Hg from solution, but above pH 4, *S. oneidensis* removes more Hg than the other two species.

3.3. XANES and EXAFS results

To probe the effect of chloride on Hg binding mechanisms with bacterial biomass, we examined Hg–biomass binding at pH 5.5 and 8.0 as a function of Hg concentration (log molalities of Hg of −5.00, −4.60, and −4.13) in the presence and absence of chloride (log molality of −3.00) using Hg L_{III} edge XANES and EXAFS. Fig. 5 shows a comparison between Hg XANES for Hg bound to the *S. oneidensis* MR-1 biomass as a function of Hg concentration in the presence and absence of chloride for both pH conditions. For comparison, XANES data for the Hg-chloride, -cysteine, and -acetate standards are also shown in Fig. 5. Hg-chloride and Hg-acetate standards have larger pre-edge features (~12,285 eV) relative to the Hg-cysteine standard (Fig. 5). Therefore, the pre-edge feature of the Hg XANES data serves as a qualitative fingerprinting approach to distinguish sulfhydryl binding from carboxyl and chloride binding environments.

Hg XANES data for the biomass samples show the smallest pre-edge feature for the sample with a log molality of Hg of −5.00, followed by the samples with Hg log molalities of −4.60 and −4.13, regardless of pH and concentration of chloride. Comparison with the standards suggests that Hg is primarily complexed with thiol groups on the bacterial biomass at the lowest Hg concentration, both in the presence and absence of chloride. Spectral features supporting this conclusion include the small pre-edge peak and the dip at 12,300 eV, similar to those

Table 1
Site concentrations and pKa values used for SCMs.

Bacteria	Site 1	Site 2	Site 3	Site 4	$[Sites]_{total}$
Site concentrations (mol sites/g bacteria)					
B. subtilis[a]	$8.1 \pm 1.6 \times 10^{-5}$	$1.1 \pm 0.36 \times 10^{-4}$	$4.4 \pm 1.3 \times 10^{-5}$	$7.4 \pm 2.1 \times 10^{-5}$	3.1×10^{-4}
S. oneidensis[b]	$8.9 \pm 2.6 \times 10^{-5}$	$1.3 \pm 0.20 \times 10^{-4}$	$5.9 \pm 3.3 \times 10^{-5}$	$1.1 \pm 0.60 \times 10^{-4}$	3.9×10^{-4}
G. sulfurreducens	$8.4 \pm 0.66 \times 10^{-5}$	$9.1 \pm 0.41 \times 10^{-5}$	$4.1 \pm 0.24 \times 10^{-5}$	$3.4 \pm 0.63 \times 10^{-5}$	2.5×10^{-4}
pKa					
B. subtilis[a]	-3.3 ± 0.2	-4.8 ± 0.1	-6.8 ± 0.3	-9.1 ± 0.2	
S. oneidensis[b]	-3.3 ± 0.2	-4.8 ± 0.2	-6.7 ± 0.4	-9.4 ± 0.5	
G. sulfurreducens	-3.4 ± 0.1	-4.8 ± 0.1	-6.5 ± 0.2	-8.8 ± 0.3	

Reported uncertainties are 1σ errors.
[a] Fein et al. (2005).
[b] Mishra et al. (2010).

present in the Hg-cysteine data (Fig. 5). Sulfhydryl binding of Hg with the bacterial biomass at low Hg concentrations is consistent with a previous study, which showed Hg binding with sulfhydryl groups on *B. subtilis* cell envelopes under similar experimental conditions (Mishra et al., 2011). The Hg–biomass data at a Hg log molality of −4.13 exhibit a larger pre-edge peak both in the presence and absence of chloride at both pH 5.5 and 8.0, similar to the Hg-acetate and Hg-chloride XANES standards. This result suggests that at the highest Hg concentration studied, Hg is bound: 1) predominantly with the lower-affinity carboxyl groups present in the biomass, 2) with chloride ligands, or 3) a combination of carboxyl and chloride ligands. The biomass sample with log molality of Hg of −4.60 exhibits a XANES pattern that is most similar to the Hg-cysteine standard, suggesting that Hg predominantly binds to the sulfhydryl groups on the cell envelope; however, it is possible that a small fraction of Hg is also bound to the lower-affinity carboxyl and/or chloride groups. It is important to note that XANES spectra of Hg which reacted *S. oneidensis* MR-1 biomass in the presence and absence of chloride at pH 5.5 and 8.0 are similar at lower Hg concentrations (Hg log molalities of −5.00 and −4.60), confirming that the binding mechanism of Hg with *S. oneidensis* MR-1 biomass does not change significantly in the presence of chloride when Hg binds preferentially with high-affinity thiol sites. XANES data of the chloride-free system are also similar to the chloride-bearing system for the sample with the highest Hg concentration at pH 5.5; however, the same samples under pH 8.0 conditions exhibit a spectral mismatch. The spectral mismatch between the chloride-bearing and chloride-free systems is better exhibited in the Fourier Transformed (FT) EXAFS data (Fig. 6).

While Hg XANES is an excellent tool for distinguishing sulfhydryl binding from carboxyl and chloride binding of Hg, Hg EXAFS can effectively distinguish between carboxyl and chloride binding. Because chloride causes more backscatter than oxygen, Hg-chloride systems are expected to have higher FT amplitudes concomitant with a larger bond distance than Hg-carboxyl systems. EXAFS FT magnitude and expanded real part data for the Hg–biomass samples as a function of Hg concentration, pH, and chloride concentration are shown in Fig. 6. Comparing the Hg XANES and EXAFS FT amplitude and peak positions of the Hg–biomass samples to those of the Hg standards, the results indicate that sulfhydryl binding dominates in the samples with Hg log molality of −5.00; that sulfhydryl binding predominantly accounts for Hg binding in the samples with Hg log molality of −4.60; and that carboxyl binding dominates in the samples with the highest Hg concentration. The lower bond distances and smaller amplitudes in the samples with Hg log molality of −4.60 relative to the Hg-cysteine and Hg-chloride standards, and the higher bond lengths and larger amplitudes relative to the Hg-acetate standard, provides evidence for this conclusion. For example, the EXAFS FT amplitude and bond length for the samples with the highest Hg concentration at pH 5.5 are similar to the Hg-acetate standard both in the presence and absence of chloride, which is consistent with the Hg XANES results described above. It is evident in Fig. 6 that the Hg EXAFS data are similar for all conditions except for the samples with the highest Hg concentration at pH 8.0. For samples with the highest Hg concentration at pH 8.0, the EXAFS FT data in the presence of chloride exhibit higher amplitudes and a small shift toward higher bond distances in the first peak position compared to the sample in the absence of chloride, providing evidence for the complexation of Hg with chloride and/or carboxyl groups on the cell envelopes. The similarities between the coordination environments for each Hg–biomass sample in the absence and presence of chloride

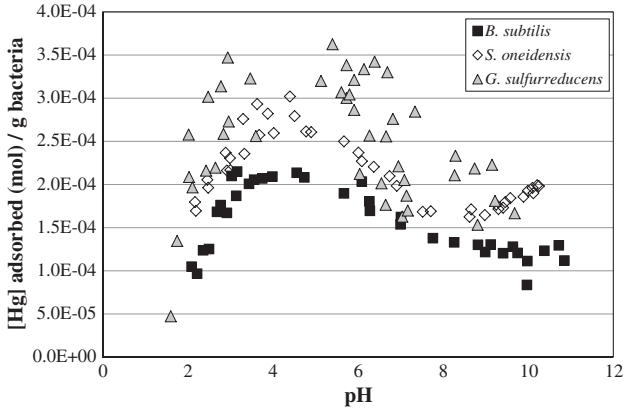

Fig. 3. Hg adsorption onto bacterial species normalized per gram of bacteria. The initial molality of Hg in the adsorption experiments is 7.41×10^{-5}.

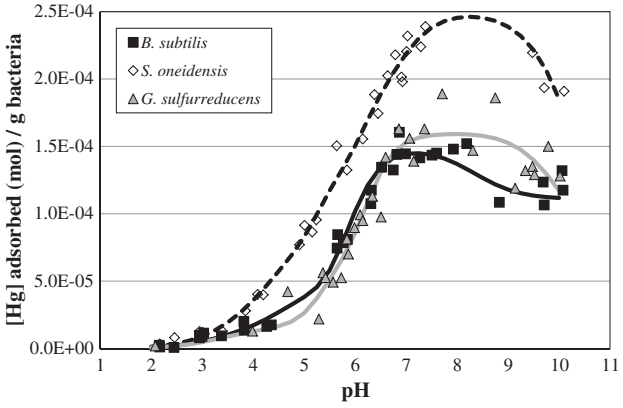

Fig. 4. Hg adsorption onto bacterial species, normalized per gram of bacteria, in the presence of chloride. The solid black curve represents the model fit for *B. subtilis*, the dashed black line represents the model fit for *S. oneidensis*, and the solid gray line represents the model fit for *G. sulfurreducens*. The initial molality of Hg in the adsorption experiments is 7.41×10^{-5} and the initial molality of Cl is 1.00×10^{-3}.

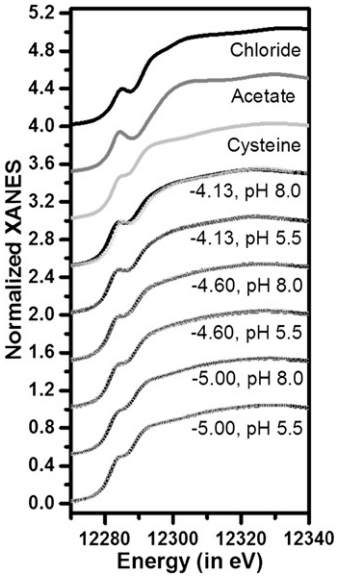

Fig. 5. Hg L_{III} edge XANES spectra for Hg bound to (from top to bottom) chloride only, acetate only, cysteine only, and *S. oneidensis* MR-1 in the absence (gray curves) and presence (black curves) of chloride (log molality of −3.00) in various combinations of Hg concentrations (reported as log molality) and pH conditions, as noted on the figure.

at the lowest Hg concentrations, as well as the differences between the Hg–biomass samples in the absence and presence of chloride at the highest Hg concentration at pH 8.0, can also be seen in the $k^2\chi(k)$ EXAFS data (Fig. S1).

Considered together, the Hg XANES and EXAFS results indicate that Hg binds predominantly to the high-affinity thiol sites followed by the lower-affinity carboxyl sites within bacterial cell envelopes in the presence and absence of chloride at low Hg concentrations regardless of the pH. However, Hg binding mechanisms with bacterial biomass are affected by the presence of chloride at pH 8.0, when Hg is primarily bound to the biomass by lower-affinity carboxyl functional groups.

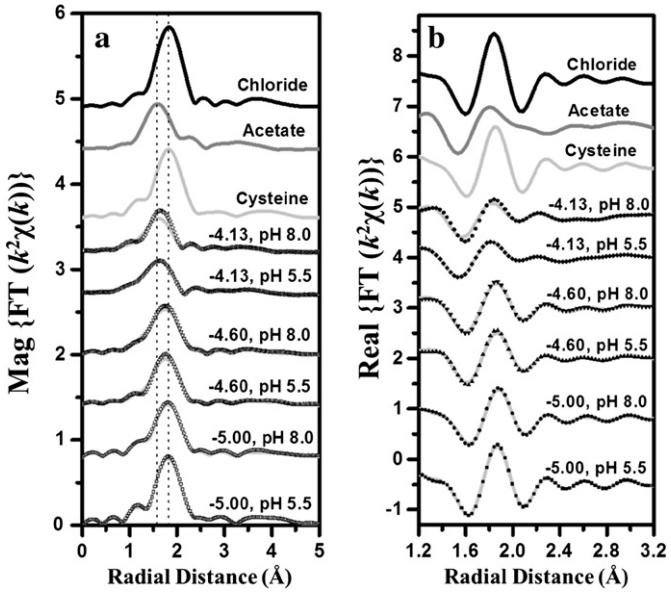

Fig. 6. Comparison of Hg L_{III} edge EXAFS Fourier Transform (FT) (a) magnitude and (b) expanded real part data for Hg binding to (top to bottom) chloride only, acetate only, cysteine only, and *S. oneidensis* MR-1 in the absence (gray curves) and presence (black curves) of chloride (log molality of −3.00) in various combinations of Hg concentrations (reported as log molality) and pH conditions, as noted on the figure.

3.4. Thermodynamic modeling

The effects of pH and chloride on the adsorption of Hg onto the bacteria studied here likely reflect both changes to the speciation of the cell envelope functional groups and changes in the aqueous Hg speciation that accompany the pH and chloride concentration changes. In order to determine the dominant adsorption reactions, it is crucial to define the speciation of Hg in solution. Aqueous Hg speciation diagrams, calculated for the experimental conditions using the aqueous complexation reactions and stability constants listed in Table S1, are depicted in Fig. 7.

In the chloride-free system, the extent of Hg adsorption that we observed is greater under all pH conditions than any of the individual binding site concentrations, meaning that under all conditions multiple site types must be responsible for the observed adsorption. For example, approximately 1.0×10^{-4} mol of Hg are adsorbed per gram of *B. subtilis* at pH 2 (Fig. 3), which represents a total concentration of adsorbed Hg of 2.1×10^{-5} M. However, the total concentration of Site 1, which deprotonates at the lowest pH of the 4 potential binding site types, is only 1.6×10^{-5} M. At pH 4.5, *B. subtilis* exhibits a maximum extent of Hg adsorption with 4.3×10^{-5} M Hg adsorbed. The total concentration of all four binding site concentrations is 6.2×10^{-5} M, again suggesting that more than one type of site is involved in Hg binding. It is unusual to observe such a high degree of site saturation by an adsorbing metal, and this behavior suggests that Hg–bacterial site stability constants are quite high. However, because individual Hg-site binding could not be isolated

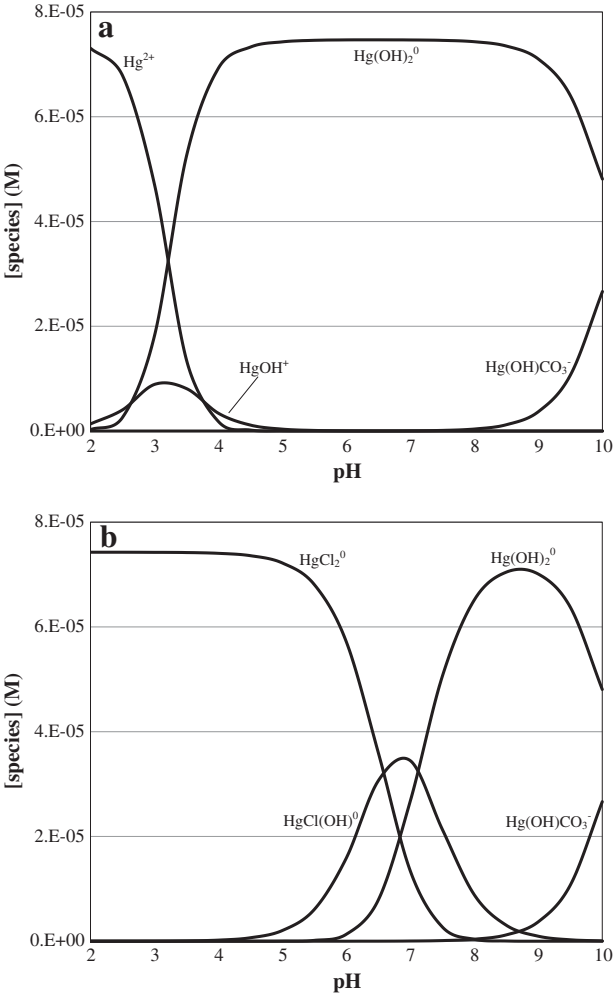

Fig. 7. Aqueous Hg speciation in the (a) absence and (b) presence of chloride under the experimental Hg and chloride concentration conditions. Only species with calculated concentrations above 0.1×10^{-6} M are shown.

under any of the experimental conditions, individual Hg-site stability constants could not be determined in the chloride-free system.

In the chloride system, we observed a stronger pH dependence for the Hg adsorption, and under low pH conditions the extent of adsorption is less than the concentration of any individual binding site type. Because Hg-chloride species dominate in the chloride experiments, and because chloride-free bacterial species are unlikely to be important under those conditions, the lack of stability constants for the chloride-free system does not hinder our ability to model the chloride system. The dramatic effect of chloride on the adsorption behavior is paralleled by the drastic change in aqueous Hg speciation with the addition of chloride (Fig. 7b). Under the conditions of our experiments and below pH 6, $HgCl_2^0$ is the dominant Hg species; however, under those pH conditions little-to-no Hg adsorption is observed, suggesting that $HgCl_2^0$ does not adsorb to bacterial functional groups strongly (Kim et al., 2004). We tested a range of models involving deprotonated sites only due to the absence of adsorption in our experiments under the low pH conditions at which protonated sites dominate the cell wall speciation. Our general approach was to model the adsorption behavior using the minimum number of adsorbed Hg species required. Because more binding site types become deprotonated with increasing pH, we modeled the low pH adsorption data first and determined whether additional adsorbed Hg species were required in order to account for the higher pH data.

Adsorption in the chloride systems increases with increasing pH above pH 4, similar to the behavior of $HgCl(OH)^0$. Daughney et al. (2002) modeled Hg adsorption onto *B. subtilis* as $HgCl_2^0$ and $HgCl(OH)^0$ binding onto a protonated bacterial site in order to account for the pH-independent adsorption that they observed under low pH conditions. In our experiments, Hg adsorption increased slightly from pH 2 to 4 for each bacterial species, under conditions where $HgCl_2^0$ dominates the aqueous Hg speciation and $R{-}A_1^{-1}$ increases in concentration due to the deprotonation of this site over this pH range. However, our EXAFS results indicate an absence of chloride in the binding environment of Hg at pH 5.5, at least for the *S. oneidensis* MR-1 sample. For this reason, we modeled the pH 2–4 data for each bacterial species with the following reaction:

$$Hg^{+2} + R{-}A_1{}^{-1} \Leftrightarrow R{-}A_1{-}Hg^{+}. \quad (5)$$

In order to determine if an additional complex is required to account for the observed Hg adsorption, we used the calculated value for the equilibrium constant for Reaction (5) to predict the adsorption behavior under higher pH conditions, assuming that only the $R{-}A_1$–Hg^+ complex controls the Hg adsorption behavior. For example, Fig. 8 depicts the fit of Reaction (5) to the data from the *B. subtilis* experiments. The predicted Hg adsorption behavior using Reaction (5) fits the experimental data well from pH 2 to 4 (the pH range used initially to constrain the K value for this reaction), but dramatically under-predicts the extent of adsorption that we observed at higher pH values. This under-prediction represents a strong evidence for the presence of an additional adsorbed Hg species or multiple species above pH 4. Again, because EXAFS provides evidence for a lack of chloride in the binding environment at pH 5.5, we concluded that Hg^{2+} is the dominant adsorbing Hg species. Therefore, in order to constrain the data between pH 4 and 5.5, we added the following reaction:

$$Hg^{+2} + R{-}A_2{}^{-1} \Leftrightarrow R{-}A_2{-}Hg^{+} \quad (6)$$

and used the pH 2–6 data from the *B. subtilis* experiments to simultaneously solve for K values for Reactions (5) and (6). Again, we use these calculated K values to predict the adsorption behavior above pH 6 (Fig. 8), and find that as expected Reactions (5) and (6) provide an excellent fit to the data up to pH 5.5. The concentrations of sites $R{-}A_1$ and $R{-}A_2$ limit the predicted extent of adsorption, which plateaus significantly below the observed extent of Hg adsorption. Following the same modeling approach, we determined that the observed Hg adsorption data from the *B. subtilis* experiments require an additional Hg–bacterial surface complex to account for the pH dependence across the pH range studied. Above pH 5.5, the EXAFS results indicate the presence of chloride in the binding environment of Hg, consistent with adsorption of $HgCl(OH)^0$, which is the dominant Hg species in solution between pH 6 and 7 (Fig. 7b), represented by the following adsorption reaction:

$$HgCl(OH)^0 + R{-}A_3{}^{-1} \Leftrightarrow R{-}A_3{-}HgCl(OH)^{-1}. \quad (7)$$

We solved for K values for Reactions (5)–(7) simultaneously with the entire dataset from the *B. subtilis* experiments, and the resulting model still under-predicts the observed extent of Hg adsorption at higher pH than those considered in the calculations to this point. Under the highest pH conditions of the experiments, $Hg(OH)_2^0$ becomes the dominant Hg species in solution, so in addition to Reactions (5)–(7), we tested models involving the adsorption of $Hg(OH)_2^0$ onto each individual deprotonated site, simultaneously solving for K values for Reactions (5), (6) and (7), as well as for the surface complex involving $Hg(OH)_2$. The only model that converged involved $Hg(OH)_2$ adsorption onto deprotonated $R{-}A_2$. Thus, the following reaction was added to our model:

$$Hg(OH)_2^0 + R{-}A_2{}^{-1} \Leftrightarrow R{-}A_2{-}Hg(OH)_2^{-1}. \quad (8)$$

We solved for K values for Reactions (5)–(8) simultaneously with the entire dataset from the *B. subtilis* experiments, and the resulting model yields an excellent fit to the data across the pH range studied (Fig. 8). Substituting adsorption of $HgCl(OH)^0$ onto another site other than site 3 in place of Reaction (8) could not account for the observed adsorption behavior. Similar modeling exercises were applied to the *G. sulfurreducens* and the *S. oneidensis* datasets (Figs. S2 and S3), and

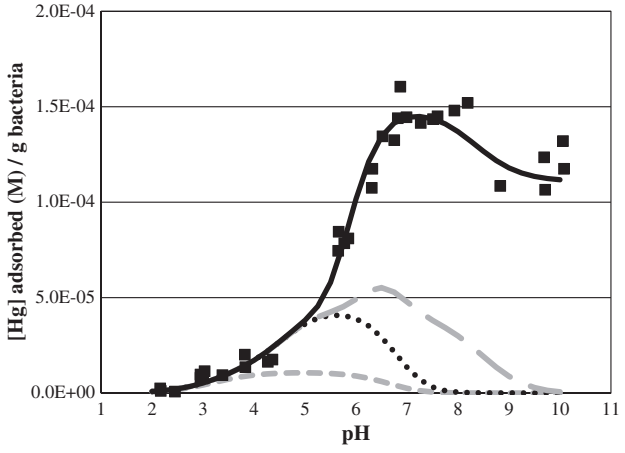

Fig. 8. Comparison of model fits (curves) to *B. subtilis* experimental data (solid squares) for the adsorption of Hg according to Reaction(s): (5) only (short-dashed gray curve); (5) and (6) (dotted black curve); (5), (6), and (7) (long-dashed gray curve); and (5) through (8) (solid black curve).

Table 2
Calculated stability constants (log K) for Hg adsorption onto bacteria.

Bacteria	Rxn (5)	Rxn (6)	Rxn (7)	Rxn (8)	Rxn (9)
B. subtilis	11.2 ± 0.2	11.8 ± 0.2	5.4 ± 0.3	6.7 ± 0.4	–
S. oneidensis	11.3 ± 0.3	12.3 ± 0.3	7.1 ± 0.2	5.0 ± 0.4	8.1 ± 0.5
G. sulfurreducens	11.3 ± 0.2	10.9 ± 0.3	6.7 ± 0.4	5.5 ± 0.3	7.7 ± 0.4

Reported uncertainties were determined by varying each average K value individually to create an adsorption envelope that encompasses 95% of the data within the pH range of influence.

the calculated K values from each of the three datasets are listed in Table 2.

For the *G. sulfurreducens* and *S. oneidensis* MR-1 models, the results are similar to the *B. subtilis* model, with Hg^{2+} adsorbing to $R{-}A_1^{-1}$ and $R{-}A_2^{-1}$, $Hg(OH)_2^0$ adsorbing to $R{-}A_2^{-1}$, and $HgCl(OH)^0$ adsorbing to $R{-}A_3^{-1}$. However, the *G. sulfurreducens* and *S. oneidensis* MR-1 data also require an additional high-pH Hg–bacterial species, and the data are best-fit with the inclusion of the following reaction:

$$HgCl(OH)^0 + R{-}A_4{}^{-1} \Leftrightarrow R{-}A_4{-}HgCl(OH)^{-1}. \quad (9)$$

The thermodynamic modeling results suggest that there is some variance between stability constants for each bacterial species. The stability constants for Reactions (5) and (9) do not vary between the bacterial species studied within experimental uncertainty, however the stability constants for Reactions (6), (7), and (8) exhibit significant variation between the species. Some of this variation certainly reflects real differences between the bacterial species. However, the differences between the K values for *G. sulfurreducens* and *B. subtilis*, which exhibit similar extents of adsorption and similar site concentrations and pKa values, may reflect the fairly large experimental uncertainty associated with the *G. sulfurreducens* data.

Though our study is similar to that of Daughney et al. (2002), both our observed Hg adsorption behaviors and the models that we use to account for that adsorption differ from those of the Daughney et al. (2002) study in some ways. Daughney et al. (2002) observed significant and relatively pH-independent adsorption below pH 4–5 and above pH 7–8, and modeled that behavior by invoking $HgCl_2^0$ and $HgCl(OH)^0$ onto protonated sites. We used the reactions and calculated stability constants from Daughney et al. (2002) to predict the extent of adsorption under our experimental conditions. The resulting predicted extents of adsorption (not shown) are inconsistent with our measurements, yielding pH independent adsorption across the pH range of our study at a level that indicates complete saturation of bacterial binding sites under all pH conditions. This result is likely due to an inconsistency between the Daughney et al. (2002) K values and their reported reaction stoichiometries, and for this reason our reported model will likely yield more accurate predictions of Hg binding behavior in a wide range of geologic and engineered systems.

4. Conclusions

In this study, we document extensive adsorption onto three different bacterial envelopes in both chloride-free and chloride-bearing systems. The experimental results demonstrate that Hg adsorption to bacterial species is dependent upon pH, chloride concentration, and bacterial surface site speciation. In the absence of a competitive ligand, such as chloride, Hg adsorption to bacterial cells does not exhibit typical metal cation adsorption behavior. Additionally, the extent of Hg adsorption onto surface sites in the absence of a ligand is extensive, with the concentration of adsorbed Hg exceeding the concentration of any individual site type under all of the pH conditions tested. In the presence of chloride, the behavior of Hg adsorption changes dramatically, with increasing adsorption as pH increases likely due to the relatively weak interaction of aqueous Hg complexes with bacterial binding sites. Thermodynamic modeling results suggest that the adsorption of Hg^{2+}, $HgCl(OH)^0$ and $Hg(OH)_2$ onto bacterial surface sites are the dominant adsorption reactions under the conditions studied, with log stability constant values ranging from −5.0 to 12.3. Our XAS results show that Hg binding to bacterial sites corresponds to sulfhydryl groups at low Hg concentrations (log molality of Hg of −5.00 and −4.60) in the presence and absence of chloride, regardless of the pH. However, the presence of chloride affects the Hg binding environment at high Hg concentrations (log molality of Hg of −4.13), when Hg is bound to lower-affinity carboxyl groups, and at high pH values. These results can be used to better understand the thermodynamics of Hg–Cl-bacterial interactions under natural geologic conditions, such as in chloride-rich seawater and bacteria-laden groundwater, and the results suggest that bacteria are likely to compete effectively with a range of other ligands present in geologic environments to control Hg distribution and speciation.

Acknowledgments

Funding for this research was provided by a grant from the Subsurface Biogeochemistry Research program within the U.S. Department of Energy. The experiments and analyses were performed at the Center for Environmental Science & Technology, University of Notre Dame. XAS measurements were obtained at the MRCAT-10-ID Beamline at the Advanced Photon Source (APS), Argonne National Laboratory. BM was supported by the Argonne Subsurface Scientific Focus Area project, which is part of the SBR Program of the Office of Biological and Environmental Research (BER), U.S. DOE under contract DE-AC02-06CH11357. We would like to thank Jennifer Szymanowski for assistance with data collection and processing.

Appendix A. Supplementary data

Supplementary data to this article can be found online at http://dx.doi.org/10.1016/j.chemgeo.2014.02.030.

References

Benoit, J.M., Gilmour, C.C., Mason, R.P., Heyes, A., 1999. Sulfide controls on mercury speciation and bioavailability to methylating bacteria in sediment pore waters. 33, 951–957.
Beveridge, T.J., 1989. Role of cellular design in bacterial metal accumulation and mineralization. Annu. Rev. Microbiol. 43, 147–171.
Beveridge, T.J., Murray, R.G.E., 1976. Uptake and retention of metals by cell walls of *Bacillus subtilis*. J. Bacteriol. 127, 1502–1518.
Beveridge, T.J., Murray, R.G.E., 1980. Sites of metal-deposition in the cell-wall of *Bacillus subtilis*. J. Bacteriol. 141, 876–887.
Blum, Bartha, R., 1980. Effect of salinity on methylation of mercury. Bull. Environ. Contam. Toxicol. 25, 404–408.
Borrok, D., Kulpa, C.F., Fein, J.B., 2004. Proton and Cd adsorption onto natural bacterial consortia: testing universal adsorption behavior. Geochim. Cosmochim. Acta 68, 3231.
Borrok, D., Turner, B.F., Fein, J.B., 2005. A universal surface complexation framework for modeling proton binding onto bacterial surfaces in geologic settings. Am. J. Sci. 305, 826–853.
Borrok, D., Aumend, K., Fein, J.B., 2007. Significance of ternary bacteria–metal–natural organic matter complexes determined through experimentation and chemical equilibrium modeling. Chem. Geol. 238, 44–62.
Chang, J.-S., Hong, J., 1994. Biosorption of mercury by the inactivated cells of *Pseudomonas aeruginosa* PU21 (Rip64). Biotechnol. Bioeng. 44, 999–1006.
Compeau, G.C., Bartha, R., 1987. Effect of salinity on mercury-methylating activity of sulfate-reducing bacteria in estuarine sediments. Appl. Environ. Microbiol. 53, 261–265.
Cox, J.S., Smith, D.S., Warren, L.A., Ferris, F.G., 1999. Characterizing heterogeneous bacterial surface functional groups using discrete affinity spectra for proton binding. Environ. Sci. Technol. 33, 4514–4521.
Daughney, C.J., Fein, J.B., 1998. The effect of ionic strength on the adsorption of H^+, Cd^{2+}, Pb^{2+}, and Cu^{2+} by *Bacillus subtilis* and *Bacillus licheniformis*: a surface complexation model. J. Colloid Interface Sci. 198, 53–77.
Daughney, C.J., Siciliano, S.D., Rencz, A.N., Lean, D., Fortin, D., 2002. Hg(II) adsorption by bacteria: a surface complexation model and its application to shallow acidic lakes and wetlands in Kejimkujik National Park, Nova Scotia, Canada. Environ. Sci. Technol. 36, 1546–1553.
Fein, J.B., Daughney, C.J., Yee, N., Davis, T., 1997. A chemical equilibrium model for metal adsorption onto bacterial surfaces. Geochim. Cosmochim. Acta 61, 3319–3328.
Fein, J.B., Martin, A.M., Wightman, P.G., 2001. Metal adsorption onto bacterial surfaces: development of a predictive approach. Geochim. Cosmochim. Acta 65, 4267–4273.
Fein, J.B., Fowle, D.A., Cahill, J., Kemner, K., Boyanov, M., Bunker, B., 2002. Nonmetabolic reduction of Cr(VI) by bacterial surfaces under nutrient-absent conditions. Geomicrobiol J. 19, 369–382.
Fein, J.B., Boily, J.-F., Yee, N., Gorman-Lewis, D., Turner, B.F., 2005. Potentiometric titrations of *Bacillus subtilis* cells to low pH and a comparison of modeling approaches. Geochim. Cosmochim. Acta 69, 1123–1132.
Fortin, D., Beveridge, T.J., 1997. Role of the bacterium *Thiobacillus* in the formation of silicates in acidic mine tailings. Chem. Geol. 141, 235–250.
Fowle, D.A., Fein, J.B., 2000. Experimental measurements of the reversibility of metal–bacteria adsorption reactions. Geochim. Cosmochim. Acta 63, 27–36.
Fuhr, B.J., Rabenstein, D.L., 1973. Nuclear magnetic resonance studies of the binding of cadmium, zinc, lead, and mercury by glutathione. J. Am. Chem. Soc. 95, 6944–6950.

Green-Ruiz, C., 2006. Mercury(II) removal from aqueous solutions by nonviable *Bacillus* sp. From a tropical estuary. Bioresour. Technol. 97, 1907–1911.
Guine, V., Spadini, L., Sarret, G., Muris, M., Delolme, C., Gaudet, J.P., Martins, J.M.F., 2006. Zinc sorption to three gram-negative bacteria: combined titration, modeling, and EXAFS study. Environ. Sci. Technol. 40, 1806–1813.
Harris, H.H., Pickering, I.J., George, G.N., 2003. The chemical form of mercury in fish. Science 301, 1203.
Hassen, A., Saidi, N., Cherif, M., Boudabous, A., 1998. Effects of heavy metals on *Pseudomonas aeruginosa* and *Bacillus thuringiensis*. Bioresour. Technol. 65, 73–82.
Kenney, J.P.L., Fein, J.B., 2011. Cell wall reactivity of acidophilic and alkaliphilic bacteria determined by potentiometric titrations and Cd adsorption experiments. Environ. Sci. Technol. 45, 4446–4452.
Kim, C.S., Rytuba, J.J., Brown, G.E., 2004. EXAFS study of mercury(II) sorption to Fe- and Al-(hydr)oxides II. Effects of chloride and sulfate. J. Colloid Interface Sci. 270, 9–20.
Ledin, M., Pedersen, K., Allard, B., 1997. Effects of pH and ionic strength on the adsorption of Cs, Sr, Eu, Zn, Cd and Hg by *Pseudomonas putida*. Water Air Soil Pollut. 93, 367–381.
Ledin, M., Krantz-Rülcker, C., Allard, B., 1999. Microorganisms as metal sorbents: comparison with other soil constituents in multi-compartment systems. Soil Biol. Biochem. 31, 1639–1648.
Lovely, D.R., Phillips, E.J.P., 1988. Novel mode of microbial energy metabolism: organic carbon oxidation coupled to dissimilatory reduction of iron or manganese. Appl. Environ. Microbiol. 54, 1472–1480.
Madigan, M.T., Martinko, J.M., Dunlap, P.V., Clark, D.P., 2009. Brock Biology of Microorganisms. Pearson Benjamin Cummings, San Fransisco.
Mishra, B., Boyanov, M.I., Bunker, B.A., Kelly, S.D., Kemner, K.M., Nerenberg, R., Read-Daily, B.L., Fein, J.B., 2009. An X-ray absorption spectroscopy study of Cd binding onto bacterial consortia. Geochim. Cosmochim. Acta 73, 4311–4325.
Mishra, B., Boyanov, M., Bunker, B.A., Kelly, S.D., Kemner, K.M., Fein, J.B., 2010. High- and low-affinity binding sites for Cd on the bacterial cell walls of *Bacillus subtilis* and *Shewanella oneidensis*. Geochim. Cosmochim. Acta 74, 4219–4233.
Mishra, B., O'Loughlin, E.J., Boyanov, M.B., Kemner, K.M., 2011. Binding of HgII to high-affinity sites on bacteria inhibits reduction to Hg^0 by mixed FeII/III phases. Environ. Sci. Technol. 45, 9597–9603.
Mo, B.-B., Lian, B., 2011. Hg(II) adsorption by *Bacillus mucilaginosus*: mechanism and equilibrium parameters. World J. Microbiol. Technol. 27, 1063–1070.
Mullen, M.D., Wolf, D.C., Ferris, F.G., Beveridge, T.J., Flemming, C.A., Bailey, G.W., 1989. Bacterial sorption of heavy-metals. Appl. Environ. Microbiol. 55, 3143–3149.
Plette, A.C.C., Benedetti, N.F., van Reimsdijk, W.H., 1996. Competitive binding of protons, calcium, cadmium, and zinc to isolated cell walls of a Gram-positive soil bacterium. Environ. Sci. Technol. 30, 3319.
Pokrovsky, O.S., Pokrovski, G.S., Shirokova, L.S., Gonzalez, A.G., Emnova, E.E., Feurtet-Mazel, A., 2012. Chemical and structural status of copper associated with oxygenic and anoxygenic phototrophs and heterotrophs: possible evolutionary consequences. Geobiology 10, 130–149.
Ravel, B., Newville, M., 2005. ATHENA, ARTEMIS, HEPHAESTUS: data analysis for X-ray absorption spectroscopy using IFEFFIT. J. Synchrotron Radiat. 12, 537–541.
Segre, C.U., Leyarovska, N.E., Chapman, L.D., Lavender, W.M., Plag, P.W., King, A.S., Kropf, A.J., Bunker, B.A., Kemner, K.M., Dutta, P, Duran, R.S., Kaduk, J., 2000. The MRCAT insertion device beamline at the Advanced Photon Source Conference Name:. Synchrotron Radiation Instrumentation: SRI99: Eleventh US National Conference Publisher: AIP Publishing 521 (1), 419–422.
Sheng, L., Szymanowski, J., Fein, J.B., 2011. The effects of uranium speciation on the rate of U(VI) reduction by *Shewanella oneidensis* MR-1. Geochim. Cosmochim. Acta 75, 3558–3567.
Small, T.D., Warren, L.A., Roden, E.E., Ferris, F.G., 1999. Sorption of strontium by bacteria, Fe(III) oxide, and bacteria-Fe(III) oxide composites. Environ. Sci. Technol. 33, 4465–4470.
Song, Z., Kenney, J.P.L., Fein, J.B., Bunker, B.A., 2012. An X-ray absorption fine structure study of Au adsorbed onto the non-metabolizing cells of two soil bacterial species. Geochim. Cosmochim. Acta 86, 103–117.
Stern, E.A., Newville, M., Ravel, B., Yacoby, Y., Haskel, D., 1995. The UWXAFS analysis package philosophy and details. Physica B 209, 117–120.
Westall, J.C., 1982. FITEQL, A Computer Program for Determination of Chemical Equilibrium Constants From Experimental Data. Version 2.0. Report 82-02 Department of Chemistry, Oregon State University, Corvallis, OR, USA.
Westall, J.C., Jones, J.D., Turner, G.D., Zachara, J.M., 1995. Models for association of metal ions with heterogeneous environmental sorbents. 1. Complexation of Co(II) by leonardite humic acid as a function of pH and $NaClO^4$ concentration. Environ. Sci. Technol. 29, 951–959.
Winfrey, M.R., Rudd, J.W.M., 1990. Environmental factors affecting the formation of methylmercury in low pH lakes. Environ. Toxicol. Chem. 9, 853–869.
Wu, S.C., Luo, Y.M., Cheung, K.C., Wong, M.H., 2006. Influence of bacteria on Pb and Zn speciation, mobility and bioavailability in soil: a laboratory study. Environ. Pollut. 144, 765–773.